

# MERCURY ZINC TELLURIDE 10.6 $\mu\text{m}$ AMBIENT TEMPERATURE PHOTODETECTORS

J. PIOTROWSKI

VIGO Ltd., P.O.B 45, 00-908 Warszawa, Poland

*(Received March 21, 1991)*

Theoretical and experimental investigations of mercury zinc telluride (MZT) ambient temperature longwavelength photodetectors are reported. The ultimate detectivities of MZT photoconductors (PC), photodiodes, photoelectromagnetic (PEM) and Demer detectors at 10.6  $\mu\text{m}$  have been calculated as a function of material composition, doping and geometry of the devices. The high-temperature longwavelength PC and PEM detectors have been fabricated from Cu-doped bulk MZT crystals grown by a modified quench/anneal technique. The measured performance has been confronted with theoretical predictions showing good overall agreement. It is concluded that the high figure of merit, stability and hardness of MZT make this material superior in comparison to mercury cadmium telluride and that it will replace the latter in application for high-temperature photodetectors. The performance of high-temperature MZT photodetectors can be further improved by the use of optical resonant cavity and optical immersion. These devices exhibit detectivity by several orders of magnitude higher than thermal detectors with subnanosecond response time, and can achieve performance comparable to that of slow thermal detectors.

PACS numbers: 72.40.+w, 72.80.Ey

## 1. Introduction

Generally, in order to achieve high sensitivity detection it is necessary to use cryogenic or at least thermoelectric cooling. This is especially important for devices operating in the far IR range. The operation of longwavelength narrow band gap semiconductor photodetectors can be successfully extended to ambient temperature provided appropriate optimization of the devices.

Ambient temperature 8–14  $\mu\text{m}$  HgCdTe photoconductor was reported for the first time by Piotrowski and other Polish workers [1–6]. Extensive experimental and theoretical studies on high-temperature photoconductors have also been

performed in the U.K. [7–8], the USA [9–11] and in Yugoslavia [12]. Due to basic physical limitations, the high-temperature photodetectors are sub-BLIP detectors, therefore improvement of their performance is a task of primary importance. Ambient temperature 10.6  $\mu\text{m}$  MCT photoconductors are at present being offered by several manufacturers [11, 13]. They find important applications in direct and heterodyne IR detection systems.

Mercury zinc telluride (MZT), due to its relative stability and high figure of merit, is a candidate to replace HgCdTe in application for high-temperature long-wavelength photoconductors [14–19]. Here we report recent achievements in the design and technology of MZT high-temperature longwavelength photodetectors.

## 2. Theoretical performance of high temperature photodetectors

### 2.1. Performance related semiconductor parameters of MZT

For calculation of the performance of photoconductors it is necessary to determine the following semiconductor properties: the band gap, intrinsic concentration, absorption coefficient and Auger recombination time. According to Toulouse et al. [18] the band gap of MZT is given by

$$E_g = -0.3 + 3.24 \times 10^{-2}x^{1/2} + 2.731x - 0.629x^2 + 0.533x^3 + 5.3 \times 10^{-4}T(1 - 0.76x^{1/2} - 1.29x) \text{ [eV]}. \quad (1)$$

The intrinsic concentration was calculated using the expression proposed by Józwiński and Rogalski [19]:

$$n_i = (3.607 + 11.37x + 6.584 \times 10^{-3}T - 3.633 \times 10^{-2}T)10^{20}E_g^{3/4} \times T^{3/2} \times \exp(-E_g/2kT) \text{ [m}^{-3}\text{]}. \quad (2)$$

The electron and light hole effective masses can be established according to the Kane band model

$$m_0/m_e^* = 1 + (2m_0P^2/3\hbar^2)[2/E_g + 1/(E_g + \Delta)], \quad (3)$$

$$m_0/m_{lh}^* = 1 - 4m_0P^2/3\hbar^2E_g, \quad (4)$$

where  $P = 8.5 \times 10^{-10}$  eV m and  $\Delta = 1$  eV. The heavy hole effective mass is

$$m_{hh}^* = 0.6m_0.$$

The electron mobility was calculated as

$$\mu_e = 1.46 \times 10^9 s/T^{2r} \text{ [cm}^2\text{/V s]}, \quad (5)$$

where  $s = (9.65 \times 10^{-2}/x)^{7.5}$ ,  $r = (9.65 \times 10^{-2}/x)^{0.6}$ .

The formula (5) is a modification of the Rosbeck et al. [20] expression for the best fit to the experimental data in the  $0.09 < x < 0.14$  range of compositions. The electron-to-hole mobility ratio  $b$  was taken equal to 100.

In narrow band gap mercury-based semiconductors and at high temperature, the Auger 1 and 7 processes are the dominant recombination mechanisms [21–22]. The intrinsic Auger 1 recombination time is

$$\tau_{A1}^i = 3.8 \times 10^{-18} \times \varepsilon_{\infty}^2 (m_0/m_e^*) (1 + m_e^*/m_h^*)^{1/2} (1 + 2m_e^*/m_h^*) \times (E_g/kT)^{3/2} \exp [(1 + 2m_e^*/m_h^*) / (1 + m_e^*/m_h^*) E_g/kT] [F_1 F_2]^2. \quad (6)$$

$F_1, F_2$  are overlap integrals of periodic Bloch functions. The value of  $[F_1 F_2]^2 = 0.2$  has been assumed to fit our experimental data for  $x = 0.10 \div 0.14$ . The high-frequency dielectric constant of MZT was approximated as

$$\varepsilon_{\infty} = 15.2 - 20.0x + 13.6x^2. \quad (7)$$

The Auger 1 and 7 recombination times are

$$\tau_{A1}^i = 2\tau_{A1}^i z^2 / (1 + z^2), \quad \tau_{A7} = 2\tau_{A7}^i / (z + z^2), \quad (8)$$

where  $z = p/n_i$ .

The ratio of intrinsic Auger 7 to Auger 1 recombination times was calculated according to [22] as

$$\Gamma = 6(1 - 5E_g/4kT) / (1 - 3E_g/2kT). \quad (9)$$

Absorption coefficient was calculated within the Kane model, taking into account the Moss–Burstein shift, according to Anderson's expressions [23]. Figure 1

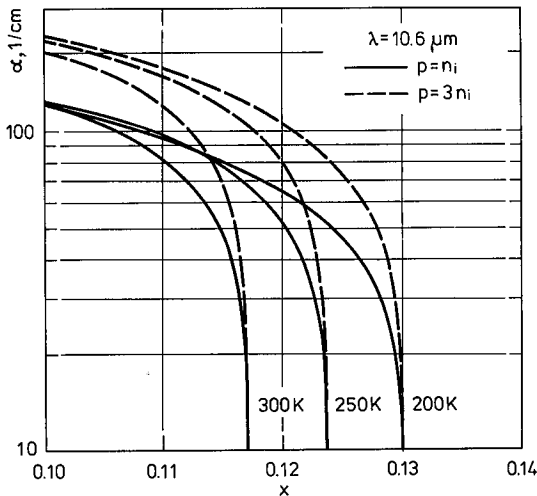


Fig. 1. Absorption coefficient of intrinsic and  $p$ -type MZT as a function of composition and temperature.

shows the calculated absorption coefficient of intrinsic and  $p$ -type MZT as a function of composition and temperature. As the figure shows,  $p$ -type doping increases absorption as a result of a reduced bandfilling effect.

## 2.2. Photoconductor parameters

The high-temperature photoconductor can be satisfactorily described by a simple model [6] in which such phenomena as sweepout effect, surface recombination and the influence of background radiation can be neglected. Let us consider a typical photoconductor as a thin flake of narrow band gap semiconductor, rectangular in shape. The resistivity of the photodetector is

$$Rv = (\lambda\eta\tau V)(b+1)/[hcn_i lwd(b/z+z)], \quad (10)$$

where  $l, w, d$  is the length, width and thickness of the photoconductor,  $\lambda$  is the wavelength of radiation, and  $\eta$  the quantum efficiency. The quantum efficiency is

$$\eta = (1-r_1)[1+r_2\exp(-\alpha d)][1-\exp(-\alpha d)]/[1-r_1r_2\exp(-2\alpha d)], \quad (11)$$

where  $r_1$  and  $r_2$  are front and backside reflectances. In the optimum case of  $r_1 = 0$ ,  $r_2 = 1$

$$\eta = 1 - \exp(-2\alpha d). \quad (12)$$

The signal-to-noise performance, or detectivity of intrinsic semiconductor photodetectors is limited by the noise caused by statistical fluctuation in charge carrier generation and recombination rates. In high-temperature photoconductors there are basically three sources of noise to be considered, the Johnson-Nyquist  $V_J$ , the generation-recombination  $V_{GR}$  and the  $1/f$  noise:

$$V_J = (4kTR\Delta f)^{1/2}, \quad (13)$$

$$V_{GR} = 2V(1+b)(\tau\Delta f)^{1/2}/[(lwdn_i)^{1/2}(b/z+z)(1/z+z)^{1/2}]. \quad (14)$$

The  $1/f$  noise can be minimized by appropriate fabrication techniques. Neglecting the  $1/f$  noise, the resulting noise voltage is

$$V_n = (V_J^2 + V_{GR}^2)^{1/2}. \quad (15)$$

The normalized detectivity is

$$D^* = R_V(lw\Delta f)^{1/2}/V_n. \quad (16)$$

When the generation-recombination noise dominates

$$D_{GR}^* = (\lambda\eta/2hc)[(1/z+z)\tau/n_id]^{1/2}. \quad (17)$$

Assuming  $r_1 = 0$  and  $r_2 = 1$

$$D_{GR}^* = (\lambda/2hc)[1-\exp(-2\alpha d)][(z+1/z)(\tau/n_id)]^{1/2}. \quad (18)$$

The last expression achieves its maximum for  $d = 0.6282/\alpha$  [12]. In this case

$$D_{max}^* = 0.451(\lambda/hc)y^{1/2}, \quad (19)$$

where

$$y = \alpha\tau(z + 1/z)/n_i. \quad (20)$$

The quantity  $\alpha\tau(z + 1/z)/n_i$  can be used as a generalized, doping-dependent figure of merit of semiconductor which determines the ultimate performance of high-temperature photoconductors at a given wavelength. For intrinsic semiconductor  $y_i$ , being equal to  $2\alpha_i\tau_i/n_i$  and to  $\alpha_i\tau_i/n_i$ , was originally introduced as the figure of merit. Figure 2 shows the generalized figure of merit of intrinsic and optimized  $p$ -type MZT for 10.6  $\mu\text{m}$  photoconductor as a function of composition. Compositions required for the best performance increase with decreasing temperature due to the temperature- band gap dependence of MZT. The  $y$  increase with  $p$ -type doping compared to the intrinsic material is a result of increasing the  $z - 1/z$ , absorption coefficient and recombination time and achieves its maximum value at  $z \approx 3$ . A further increase of doping results in a decrease of  $y$  mainly due to the rapid decrease of the Auger 7 recombination lifetime. It should be noted that the calculated and measured values for intrinsic material at 300 K are higher compared to the ones calculated by Spears [9].

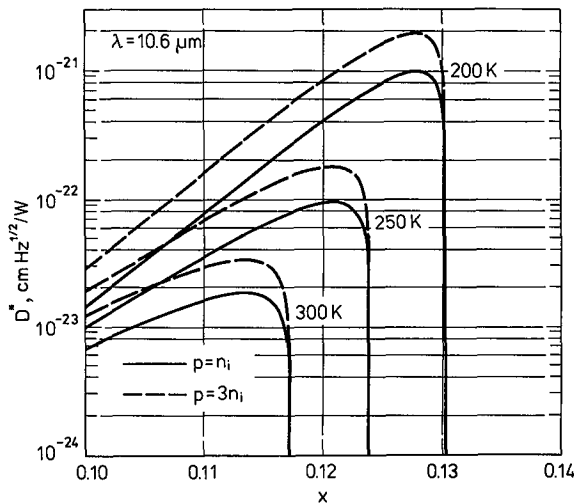


Fig. 2. The figure of merit of intrinsic and  $p$ -type ( $z = 3$ ) MZT for 10.6  $\mu\text{m}$  photoconductors as a function of composition and temperature.

Figure 3 shows basic parameters of uncooled 10.6  $\mu\text{m}$ -optimized photoconductors as a function of doping. In the calculations, a bias power density of 1  $\text{W}/\text{mm}^2$  was assumed, the value achievable in an optimized heat dissipation design.

As Fig. 4 shows, the normalized detectivity increases with bias at low bias when thermal noise prevails. At high bias the detectivity achieves the generation-recombination noise limit. A very good bias power dissipation is required to achieve

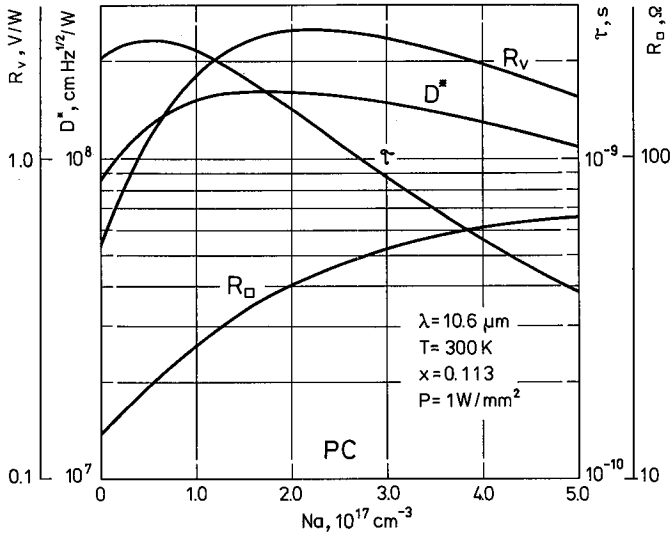


Fig. 3. Properties of ambient temperature 10.6  $\mu\text{m}$ -optimized photoconductor as a function of doping.

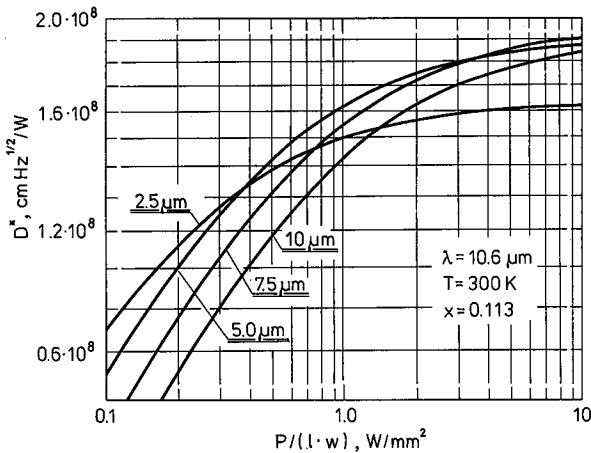


Fig. 4. The calculated normalized detectivity of ambient temperature 10.6  $\mu\text{m}$  photoconductor as a function of bias power density for various thicknesses.

this maximum performance. This may be difficult to realize in practice, however. It should be noted that the optimum composition, doping and detector thickness depends on the bias power density. Detectivity of about  $1.6 \times 10^8 \text{ cm Hz}^{1/2}/\text{W}$  can be achieved in optimized devices ( $x = 0.113$ ,  $z = 3$ ,  $d = 5 \mu\text{m}$ ), with  $1 \text{ W}/\text{mm}^2$  bias power dissipation, while the generation-recombination noise limit of performance

is  $\approx 2 \times 10^8 \text{ cm Hz}^{1/2}/\text{W}$ . Cooling to 200 K increases detectivity by one order of magnitude (Fig. 5); this, however, is accompanied by an increase of the response time.

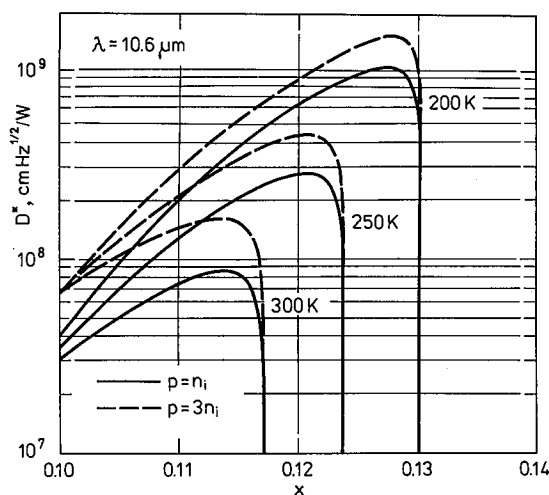


Fig. 5. The calculated normalized detectivity of the optimized 10.6  $\mu\text{m}$  photoconductors as a function of composition and temperature. The vertical line shows values measured at 300 K.

### 2.3. Photoelectromagnetic detector parameters

The photoelectromagnetic effect has also been used for ambient temperature MZT 10.6  $\mu\text{m}$  photodetectors [6, 24–30]. The diffusion length in the narrow band gap MZT is small ( $L_d < 2 \mu\text{m}$ ) while the absorption of 10.6  $\mu\text{m}$  radiation is relatively weak ( $\alpha \approx 1000/\text{cm}$ ). In such cases, the radiation is uniformly absorbed within the diffusion length and a large difference in the surface recombination velocities is necessary for a good response of PEM detector. The voltage responsivity and detectivity has been calculated using the generalized theory of PEM effect given by Lile [24], assuming the optimum case of 0 and 1 reflection coefficients at the front and rear surfaces, respectively. As no biasing is applied to the PEM detector, the thermal Johnson–Nyquist noise is the only noise. Figure 6 shows the calculated detectivity as a function of material composition for detectivity-optimized doping, thickness and magnetic field. The maximum achievable voltage responsivities and detectivities of uncooled 10.6  $\mu\text{m}$  device are of about 0.5 V/W (for 1mm wide device) and  $3.5 \times 10^7 \text{ cm Hz}^{1/2}/\text{W}$ , respectively and the detectivity increases by a factor of 9 at 200 K. As Figs. 7 and 8 show, the optimum performance of the uncooled device is achievable with  $p$ -type material, ( $Na = 2.4 \times 10^{17} \text{ cm}^{-3}$ ) and with a magnetic field of 2 T. The response time of detectivity-optimized devices is of about 1 ns. In a high frequency design, the response time below 100 ps can be achieved, with some expense of performance.

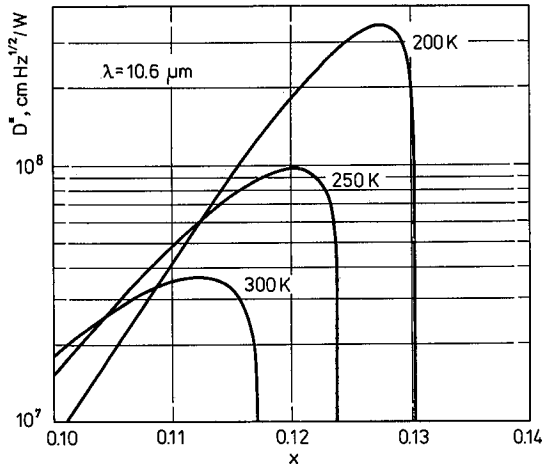


Fig. 6. The normalized detectivity of  $10.6 \mu\text{m}$  PEM detectors as a function of composition and temperature.

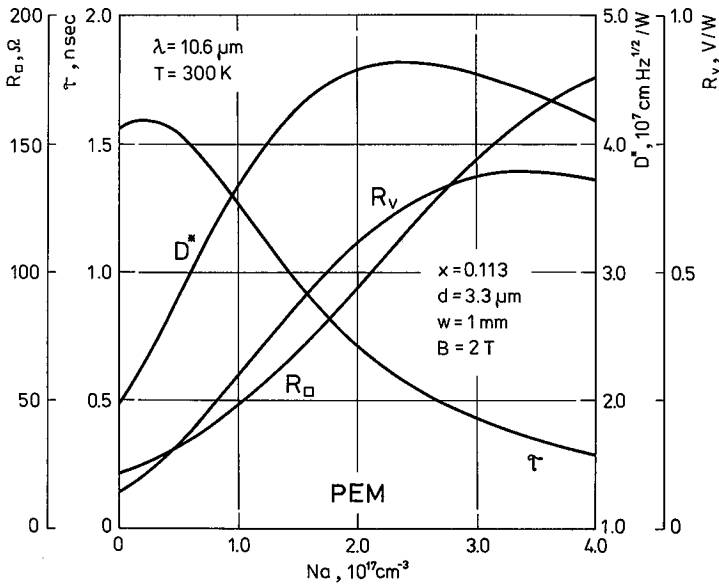


Fig. 7. Parameters of  $10.6 \mu\text{m}$ -optimized PEM detectors as a function of acceptor doping.

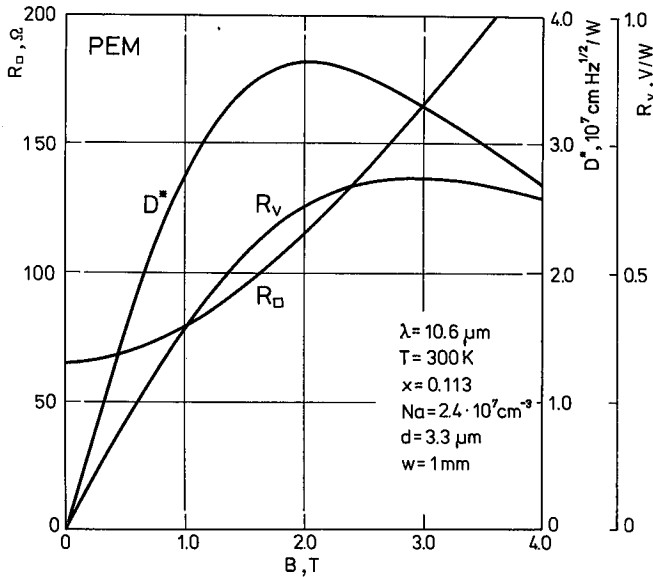


Fig. 8. Parameters of 10.6  $\mu\text{m}$ -optimized uncooled PEM detectors as a function of magnetic field.

#### 2.4. Dember detectors

The diffusion photovoltage (Dember) effect results from diffusion of photogenerated carriers [31–33]. Two conditions are to be met for generation of the photovoltage: the distribution of photogenerated carriers should be ununiform and the diffusion coefficients of electrons and holes must be different. The gradient usually results from nonuniform optical generation and from a difference in surface recombination velocities at the front and back surfaces of the device. The Dember effect electrical field restrains the electrons with higher mobility, while holes are accelerated, thus making both fluxes equal. The best performance is achievable for a thickness of the device of the order of the diffusion length and for low recombination velocity at the front and high at the back surface of the device.

The Dember effect detectors can be analyzed by solving the transport and continuity equations [31]. Figure 9 shows the calculated normalized detectivity of 10.6  $\mu\text{m}$  MCT Dember detectors as a function of composition and temperature. Detectivities as high as  $2.3 \times 10^8 \text{ cm Hz}^{1/2}/\text{W}$  and  $2.1 \times 10^9 \text{ cm Hz}^{1/2}/\text{W}$  are predicted for optimized 10.6  $\mu\text{m}$  devices at 300 and 200 K, respectively. Figure 10 shows the doping dependence of the calculated normalized responsivity, detectivity and response time for uncooled 10.6  $\mu\text{m}$  MCT Dember detector with detectivity-optimized thickness. The best performance is achieved in  $p$ -type doped materials. The calculated detectivity of 200–300 K Dember detectors is higher compared to that of photoconductors operated at the same conditions. Very low

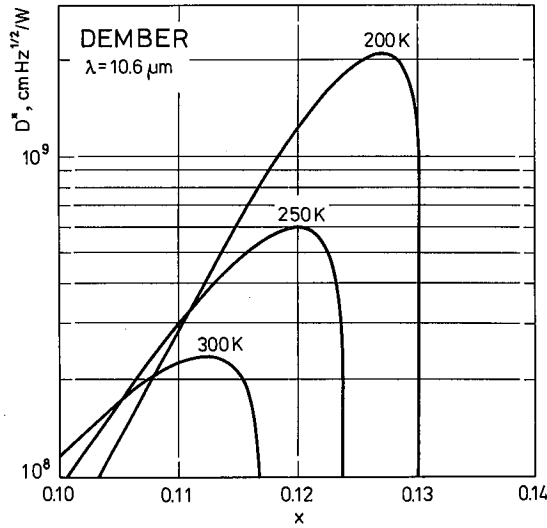


Fig. 9. The normalized detectivity of 10.6 μm Dember detectors as a function of composition and temperature.

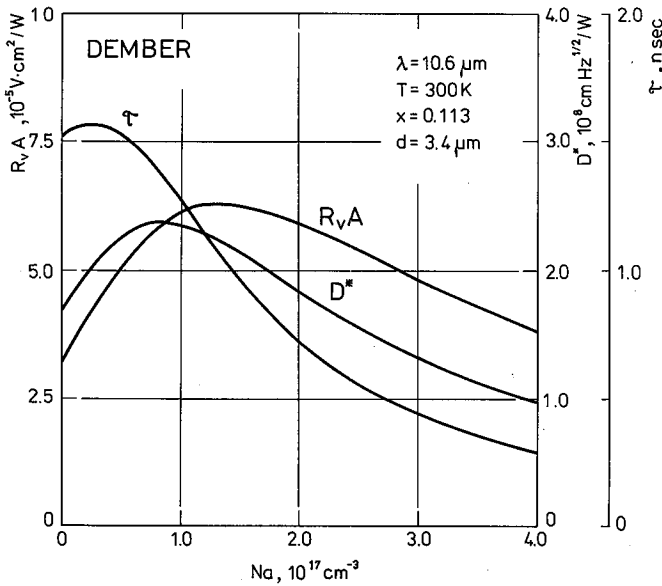


Fig. 10. Properties of 10.6 μm-optimized uncooled Dember detectors as a function of doping.

resistances, low voltage responsivities and noise voltages well below the noise level of the best amplifiers pose serious problems in achieving the potential performance, however. For example, uncooled 10.6  $\mu\text{m}$  devices with size  $50 \times 50 \mu\text{m}^2$  will have a resistivity of  $0.15 \Omega$  and a noise voltage of  $50 \text{ pV/Hz}^{1/2}$ . There are some possible ways to overcome this difficulty. The one is a connection of small area Dember detectors in series. For example, to obtain reasonable resistivity ( $\sim 50 \Omega$ ) in a  $1 \text{ mm}^2$  total area sensitive element of uncooled 10.6  $\mu\text{m}$  detector, it is necessary to divide its area into 400  $50 \times 50 \mu\text{m}^2$  elements, connected in series with low resistivity interconnection. Such a device is feasible with methods of modern microelectronics.

The response time of detectivity optimized devices is of about 1 ns, decreasing with  $p$ -type doping, at some expense in performance. High frequency optimized Dember detectors should be prepared from strongly doped material and their thickness should be kept low. For example, for detectors with  $Na = 5 \times 10^{17} \text{ cm}^{-3}$  and  $d = 2 \mu\text{m}$ ,  $\tau_r \approx 50 \text{ ps}$ . Another possible limitation of the response time, the  $RC$  constant is not important due to the low resistivity and low capacity of Dember detectors.

### 2.5. Photodiodes

Photodiodes have been extensively used primarily as LN cooled high speed detectors of  $\text{CO}_2$  laser radiation in the direct and heterodyne mode and in thermal imaging systems in 3–5 and 8–14  $\mu\text{m}$  atmospheric band. These devices have also a potential for operation at elevated temperatures. The calculated performance of photodiodes is slightly lower compared to that of photoconductors but higher compared to that of PEM detectors.

The low normalized resistivity and responsivity seriously restrict the usefulness of conventional photodiodes to the short and medium wavebands. For example, the resistivity of a  $100 \times 100 \mu\text{m}$  10.6  $\mu\text{m}$  photodiode operated at 300 and 200 K is equal to about 0.5 and  $14 \Omega$ , respectively. Under such conditions, the noise of amplifiers is above the diode noise. This enables to achieve the potential detectivity of the device and this is the reason why photoconductors and PEM detectors are at present the most frequently used photodetectors for high-temperature applications.

## 3. Photodetectors fabrication and measured performance

The ambient temperature photodetectors have been fabricated from bulk, Cu-doped MZT crystals grown by the quench/anneal technique [34]. Figure 11 shows the structure of the high-temperature photoconductors and PEM detectors. The devices are thin flakes of narrow band gap semiconductors supplied with electrodes and fixed to a heat conductive substrate. The preparation of the devices includes: deposition of a ZnS and gold layer on a carefully polished wafer of HgZnTe, epoxing the wafer to silicon or sapphire substrate, polishing the wafer to its final thickness of about  $5 \mu\text{m}$ , delineation of active areas and metallization for

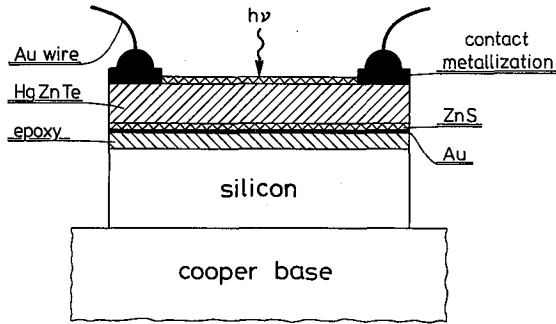


Fig. 11. The structure of MZT photoconductors and PEM detectors.

contact electrodes. The thickness of the epoxy layer should be as low as  $1\ \mu\text{m}$  for good heat dissipation. In the case of PEM detectors, the back surface of the polished HgZnTe wafer is subjected to a treatment for a high surface recombination velocity.

The sensitive elements are housed in high-frequency casings. The PEM elements are mounted in a housing which incorporates a miniature permanent magnet. The use of rare earth magnetic materials allows to obtain a magnetic field above 1 T.

The above-average measured detectivity of the ambient temperature photodetectors is shown in Figs. 2 and 5. The measured performance of PC and PEM detectors is many orders of magnitude higher compared to any pyroelectric detectors with subnanosecond response time and photon drag detectors. A comparison of the experimental results with the theory shows that it is still possible to improve the performance significantly.

#### 4. Possibilities of further improvement of the performance

##### 4.1. Optical immersion

The optical immersion of detectors into high refraction index hemispherical or hyperspherical lenses reduces the image size by a factor dependent on  $n$ , the refraction coefficient of the lens. This size is reduced by a factor equal to  $n^2$  if the detector is placed in the center of a hemispherical lens, or by  $n^4$  if the detector is placed at the first Weierstrass point of a hyperhemispherical lens, extending beyond the centre of the sphere. With optical immersion a large detector is replaced by a smaller one that has the equivalent apparent optical area. The immersion increases the normalized detectivity by a factor equal to  $n$  in the case of hemispherical immersion, and by  $n^2$  in that of hyperhemispherical immersion [35–36].

Despite the lower increase of detectivity, hemispherical immersion is frequently used for the following reasons. The hemispherical lens may be included in the existing optical system causing no change in the position of the focal plane

and introducing no restrictions on the system numerical aperture. A hyperspherical lens will introduce an image shift that will increase with the lens radius, and the maximum numerical aperture of the host system is determined by the refraction coefficient. The higher  $n$ , the slower the optics. The significant reduction of the electrical area of the immersed detectors compared to the optical one results in a significant reduction (by a factor of  $n^2$  or  $n^5$ ) of the bias power. This is an important advantage in the high temperature photoconductors, which for the best performance, require high biasing. For the best result, the materials for immersion lenses should have a high refraction coefficient and low absorption at the wavelengths of interest. Reflection losses can be prevented by the use of a suitable antireflection coating of the lenses. Germanium ( $n = 4$ ) is typically used for immersion lenses which can operate both in the 3–5  $\mu\text{m}$  and 8–14  $\mu\text{m}$  bands. Recently, monolithic optically immersed high-temperature photodetectors have been reported [37], in which the lenses were formed in substrates of detector epilayer.

Optical immersion seems to be very promising for photodiodes and Dember detectors. Apart from the usual  $n$  or  $n^2$  gain, immersion results in a large increase in resistivity. For example, the resistivity increases by a factor of  $n^4 = 256$  with the use of Ge hyperimmersion lens, compared to that of a conventional device of the same apparent area, highly easing matching to low noise preamplifiers.

#### 4.2. Resonant optical cavity

The voltage responsivity and detectivity increase with decreasing thickness of a photoconductor if the quantum efficiency remains high. The effective absorption of radiation in thin photoconductors can be increased using the interference effect to set up the resonant optical cavity. The structure of the resonant cavity consists of a semiconductor flake, is sandwiched between two dielectric layers, with the rear dielectric layer surface covered with a highly reflective coating. All the surfaces must be sufficiently flat. It has been shown [38] that the use of an optical resonant cavity can improve the performance of photoresistors by a factor of 2.5 and an improvement by a factor of  $\approx 5$  is possible for photodiodes, Dember and PEM detectors.

#### 4.3. Non-equilibrium devices

Recently, British workers have shown that the performance of high-temperature longwavelength photoresistors and photodiodes can be improved with the use of exclusion and extraction effects at l-h or at heterojunction contacts [39–41], making possible to achieve BLIP performance at near room temperature. The practical realization of such devices will require well established epitaxial technology, but the first practical non-equilibrium (Hg,Cd)Te devices based on existing technology have already been demonstrated.

#### 4. Conclusions

1. The figure of merit, responsivities, response time and ultimate performance of 200–300 K, longwavelength MZT photoconductors, photodiodes, Dember and PEM detectors have been calculated as a function of temperature, composition, doping and other factors. It has been shown that the ambient temperature 10.6  $\mu\text{m}$  photodetectors, having subnanosecond response time can achieve performance of the slow thermal detectors.
2. The high temperature MZT photoconductors and PEM detectors have been fabricated from Cu-doped, bulk MZT crystals grown by the quench/anneal technique and characterized.
3. The optimized "conventional" ambient temperature 10.6  $\mu\text{m}$  MZT photoconductor and Dember detectors can achieve detectivity higher than  $10^8 \text{ cm Hz}^{1/2}/\text{W}$ .
4. The performance of ambient temperature photodetectors can be improved using the principles of optical resonant cavity and optical immersion. Immersion also facilitates matching of photodiodes and Dember detectors to low-noise electronics, enabling to achieve their potential performance. Such devices with subnanosecond response time can surpass the performance of the best slow thermal detectors.
5. A further improvement of performance is possible by the use of non-equilibrium effect at the l-h or at heterojunction contacts.
6. The combination of all these methods may eventually allow to achieve the BLIP performance at near ambient temperature.

#### References

- [1] J. Piotrowski, *Properties of HgCdTe Layers*, Ph.D. Thesis, Military Academy of Sciences, Warsaw 1972, (in Polish).
- [2] J. Piotrowski, *Electron Technol.* **5**, 87 (1972).
- [3] E. Igras, Z. Nowak, T. Persak, J. Piotrowski, in: *Proc. 6th Symp. of IMEKO Technical Committee on Photon Detectors, Siofok-Budapest 1987*, IMEKO Secretariat H-1371, Budapest 1974, p. 221.
- [4] W. Galus, T. Persak, J. Piotrowski, *Infrared Phys.* **19**, 649 (1979).
- [5] W. Galus, F. Perry, *Laser Focus*, **20**, 76 (1984).
- [6] J. Piotrowski, A. Rogalski, *Półprzewodnikowe detektory podczerwieni WNT*, Warszawa 1985 (in Polish) and related papers cited therein.
- [7] C.T. Elliott, *Handbook on Semiconductors* **4**, 727 (1981).
- [8] F.A. Capocci, A.T. Harker, M.C. Wilson, D.E. Lacklison, F.E. Wray, in: *Proc. 2nd Inter. Conf. on Advanced Infrared Detector and Systems*, IEE, London 1983, p. 40.
- [9] D.L. Spears, in: *Proc. of IRIS Specialty Group on IR Detectors*, San Diego 1982, p. 1.
- [10] D.L. Spears, in: *Proc. of IRIS Active Systems*, San Diego 1984, p. 331

- [11] T.S. Wong, *Lasers and Applications*, 2, 59 (1987).
- [12] Z. Djuric, J. Piotrowski, Z. Jaksic, Z. Djinovic, *Electron. Lett.* 24, 1590 (1988).
- [13] VIGO Ltd., commercial data sheets, Warsaw (Poland).
- [14] A. Sher, A.B. Shen, W.E. Spicer, C.K. Shih, *J. Vac. Sci. Technol. A* 3, 105 (1985).
- [15] A. Sher, D. Eger, A. Zemel, *Appl. Phys. Lett.* 46, 59 (1985).
- [16] K. Adamiec, A. Maciak, Z. Nowak, J. Piotrowski, *Appl. Phys. Lett.* 54, 143 (1989).
- [17] P. Brogowski, H. Mucha, J. Piotrowski, *Phys. Status Solidi A* 114, K37 (1989).
- [18] B. Toulouse, R. Granger, S. Rolland, R. Triboulet, *J. Phys.* 48, 247 (1987).
- [19] K. Jóźwikowski, A. Rogalski *Infrared Phys.* 28, 101 (1988).
- [20] J.P. Rosbeck, R.E. Star, S.L. Price, K.J. Riley, *J. Appl. Phys.* 53, 6430 (1982).
- [21] P.E. Petersen, *Semiconductors and Semimetals* 18, 121 (1981).
- [22] T.N. Casselman, *J. Appl. Phys.* 52, 848 (1981).
- [23] W.W. Anderson, *Infrared Phys.* 20, 363 (1980).
- [24] D.L. Lile, *Phys. Rev. B* 8, 4708 (1973).
- [25] W. Galus, M. Grudzien, T. Niedziela, J. Piotrowski, in: *Proc. 9th Symp. of IMEKO Tech. Comm., Visegrad 1980*, IMEKO Secretariat, Budapest 1980 p. 223.
- [26] T. Niedziela, *Design of MCT PEM Detectors*, Ph.D. Thesis, Military Academy of Technology (WAT), Warsaw 1983.
- [27] D. Genzow, A. Jóźwikowska, K. Jóźwikowski, T. Niedziela, J. Piotrowski, *Infrared Phys.* 24, 21 (1984).
- [28] K. Jóźwikowski, M. Nowak, J. Piotrowski, *Infrared Phys.* 24, 371 (1984).
- [29] T. Niedziela, J. Piotrowski, *J. Tech. Phys.* 27, 25 (1986).
- [30] M. Nowak, *Prog. Quantum Electron.* 11, (1987).
- [31] J. Auth, D. Genzow, K.H. Herrmann, *Photoelektrische Erscheinungen*, Akademie Verlag, Berlin 1977.
- [32] T. Niedziela, J. Piotrowski, *J. Tech. Phys.* 28, 173 (1987).
- [33] T. Niedziela, J. Piotrowski, *J. Tech. Phys.* 28, 275 (1987).
- [34] Z. Nowak, J. Piotrowski, J. Rutkowski, *J. Cryst. Growth* 89, 237 (1988).
- [35] J.E. Slavek, H.H. Randal, *Infrared Phys.* 21, 105 (1981).
- [36] I.C. Carmichael, A.B. Dean, D.J. Wilson, *Advances Infrared Detector and Systems*, IEE, London 1983, p. 45.
- [37] M. Grudzień, J. Piotrowski, *Infrared Phys.* 29, 251 (1989).
- [38] T. Niedziela, (to be published).
- [39] T. Ashly, T.C. Elliott, *Electron Lett.* 21, 451 (1985).
- [40] T. Ashly, C.T. Elliott, A.T. Harker, *Infrared Phys.* 26, 303 (1986).
- [41] C.T. Elliott, in: *Proc. Symp. on Narrow Band Gap Semiconductors Gaithersburg*, Eds. D.G. Seiler, C.L. Litter, Bristol, New York 1990, p. S-30.